Int. J. Electrochem. Sci., 11 **(2016)** 5735 – 5752, doi: 10.20964/2016.07.82

International Journal of
ELECTROCHEMICAL
SCIENCE
www.electrochemsci.org

Self-healing Passivation of Antimicrobial Iron oxide Nanoparticles for Epoxy Nanocomposite Coatings on Carbon Steel

Ayman M. Atta[1,2,*], *Ashraf M. El-Saeed*[1], *H. I. Al-Shafey*[1] *and Gamal A. El-Mahdy*[3]

[1] Petroleum Application Department, Egyptian Petroleum Research Institute, Nasr City 11727, Cairo, Egypt.
[2] Chemistry department, college of science, King Saud University, Riyadh 11451, Saudi Arabia.
[3] Chemistry Department, Faculty of Science, Helwan University, Helwan, Egypt.
[*]E-mail: aatta@ksu.edu.sa

Received: 14 April 2016 / *Accepted:* 19 May 2016 / *Published:* 4 June 2016

Self-healing smart nanomaterials are fast responsive materials that can be used to repair organic coating defects. In this work, the ability of smart nanomaterials based on iron oxide nanoparticles capped with Myrrh to form protective films for epoxy nanocomposites defect in corrosive medium is investigated. The functionalization of iron oxide nanoparticles with Myrrh, their crystal shape and morphologies were confirmed by advanced analyses. The mechanical characteristics of iron oxide epoxy nanocomposites such as impact strength, bending and abrasion resistances and their adhesion performances with steel were measured using different iron oxide nanoparticles contents ranged from 0.1 to 10 Wt%. The corrosion resistances of epoxy iron oxide nanocomposites were measured using salt spray resistance and electrochemical methods to investigate the barrier properties and self-healing performance of the epoxy coatings without and with the additions of iron oxide nanoparticles.

Keywords: Iron oxide; nanoparticles; epoxy; nanocomposites; coatings; corrosion.

1. INTRODUCTION

Self-healing smart materials have been recently attracted the attention as high performance advanced materials that would be economically reasonable, durable and the paradigm of damage prevention during use of materials. These materials are nanomaterials, composites, functional materials, ceramics and shape memory alloys [1-4]. The self healing mechanisms can be classified to be automatic and non-autonomic when they did not require and required additional energy, respectively. Moreover, self-healing polymer systems were divided to be smart and re-mendable materials depend on chemical nature of healing processes [5, 6]. However, the healing agents were

generally encapsulated and embedded into composite matrixes. They were released into cracks or damaged composites by capillary effect and heal the cracks. They were single components such as cyanoacrylate [7, 8] and polyvinyl acetate [9] or two-component ones. There are different proposed mechanisms, such as molecular inter-diffusion, UV-photo-induced healing and recombination of polymer chain ends, living polymers and self-healing via reversible bond formation, used to explain the healing of polymeric materials [9]. It was also reported that a novel pressure delivery mechanism explained the self- healing of epoxy nanocomposite using poly[ethylene-co-methacrylic acid] (EMAA) particles [11-13]. Recently, nanomaterials attracted great attention and applied as fascinating self-healing materials for different organic coating composites due to their versatile functions high surface area, and enhanced transport property offer the time and saving the materials [14, 15]. These materials were applied as nanotubes, nanocapsules, nanofibers and nanorods [14-16]. Moreover, these materials used to fill the cracks and without breaking and rejoining of polymer chains.

Epoxy resins have been reported as commercially applied materials that used as organic coating to protect steel from corrosion and mechanical damages [17]. One of epoxy drawbacks that would fail the epoxy coats was non- detected damage or crack which produced from high crosslinked epoxy networks. These damages required repair plan systems to protect the coating failures. In this respect, micro/nanocapsules as nanocontainers can be used to with a liquid healing agent to repair epoxy organic coatings [18]. The carbon nanotubes, layered nanoclay, zirconia, hallow silica, titania, silver nanomaterials were reported as nanocontainers self- healing repair for epoxy coatings [19, 20]. The important aspects to design self-healing nanomaterials were attributed to their high compatibility with coatings and sensitivity to environmental changes such as pH, ionic strength, temperature, magnetic field or electromagnetic field. In this respect, it was previously reported that the magnetite and maghemite have great ability to form passive protective layers that can protect steel from atmospheric corrosions. The main problems to apply these materials produced from their lower adhesion to steel surfaces. In our previous works [21-25], we succeeded to prepare self- assembled magnetite nanocomposites at steel surfaces which used to protect steel from corrosion in aggressive acidic medium. The aim of the present work is to apply oxygen and salt sensitive magnetite nanoparticles as smart self-healing via passivation materials for damaged epoxy nanocomposite at steel surfaces. The magnetite/epoxy nanocomposites claimed to react with oxygen to undergo passivation at the steel surfaces when any damages or pinholes formed in the salt water. The effect of magnetite/maghemite nanoparticles on self- healing activity of damaged epoxy coatings at the steel surfaces was investigated by evaluation mechanical properties, salt spray and corrosion resistance tests. The self-healing efficiencies of damaged epoxy were evaluated by scanning electron microscope (SEM) and X-ray powder diffraction (XRD) of damaged area. The corrosion inhibition efficiencies were measured using different electrochemical techniques.

2. EXPERIMENTAL

2.1. Materials

Two component solvent free epoxy resin with polyamine curing agent (SigmaGuard ^{TM} CSF 650) produced by Sigma Coatings, SigmaKalon group was used as organic coating for carbon steel.

The mixing ratio between epoxy and polyamine hardner by volume was 4:1. Myrrh gum is a commercial polysacharide natural product with yellowish red color. The soluble fraction of Myrrh gum was extracted using ethanol/water (1:1 volume %). Anhydrous ferric chloride ($FeCl_3$), potassium iodide, and ammonium hydroxide (28%) were obtained from Aldrich Chemical Co. and used as reagent for preparation of iron oxide nanoparticles. Carbon steel specimens having chemical composition (wt.%): 0.14% C, 0.57% Mn, 0.21% P, 0.15% S, 0.37% Si, 0.06% V, 0.03% Ni, 0.03% Cr was used and blasted before apply the epoxy resins as organic coatings.

2.2. Preparation of irom oxied Myrrh capped nanoparticles

The method used to prepare iron oxide nanoparticles capped with Myrrh was discussed briefly to produce magnetite nanoparticles [26]. In brief, 13.2 g (0.08 mol) of potassium iodide dissolved in 50 ml of distilled water was mixed with 40 g of anhydrous $FeCl_3$ solution in 300 ml under stirring at room temperature. The iodine precipitate was formed as product of reaction. The solution was heated slowly up to 50 ^{o}C. Soluble fraction (ethanol/water) of Murrh (5 g in 100 ml of ethanol: water solvent 1:1 vol %) was added dropwise to the reaction mixture. Ammonia solution (200ml of 28 %) was added at the same time at temperature 50 ^{o} C. The reaction temperature was kept at this temperature under stirring for 4 hrs. The dispersed iron oxide nanoparticles were isolated by ultracentrifuge at 8,000 rpm for 30 minutes. The precipitate was washed with ethanol and air dried without heating to produce iron oxide capped with Myrrh nanoparticles having yield percentage of 99.5 %. This product was abbreviated as iron oxide / Myrrh / I_2.

The same procedure was repeated except that the iodine precipitate was removed from reaction mixture before adding Myrrh and ammonia solution. The products of reaction was designated as iron oxide / Myrrh nanoparticles.

2.3. Coating of steel with epoxy/iron oxide nanocomposite

The blasted and cleaned panels were coated with two component epoxy as blank and with epoxy / iron oxide nanocomposites. The iron oxide contents were 0.1, 1 and 10 Wt % related to the epoxy resin and hardener contents. The iron oxide nanoparticles capped with Myrrh was mixed with epoxy resin by ultra-sonication rod with power of 25 % for 25 min. The epoxy resins were mixed with amine based hardener at mixing ratio 4:1 of epoxy : hardener. The mixtures were applied on the steel panels by means of a conventional spraying to obtain dry film thickness (DFT) of 100 μm after curing at room temperature for 6 hrs. The same procedure was used without adding iron oxide nanoparticles as blank for evaluating the mechanical properties and corrosion resistance tests.

2.4. Characterization of Epoxy/iron oxide nanocomposites

2.4.1 Capped iron oxide nanoparticles

The chemical structure of iron oxide nanoparticles and their composites with epoxy was determined using FTIR model Nicolet FTIR spectrophotometer using KBr in a wave number range of 4000–400 cm^{-1} with a resolution accuracy of 4 cm^{-1}.

Transmission electron microscopy (TEM; model JEOL JEM-2100F; JEOL, Tokyo, Japan) was used to study the morphologies of nanoparticles at an acceleration voltage of 200 kV.

The surface morphologies of iron oxide nanoparticles and their composites with epoxy were investigated using scanning electron microscopy (SEM, model JSM-T 220A, JEOL) at an accelerated voltage 200 kv.

X-ray powder diffraction (XRD) patterns were recorded using a D/max 2550 V X-ray diffractometer (X'Pert, Philips, Eindhoven, The Netherlands).

2.4.2. Antimicrobial activity of iron oxide nanoparticles

Gram-positive and negative Bactria strains based on Escherichia coli ATCC 8739, Staphylococcus aureus ATCC 6538, Bacillus subtilis ATCC 6633 and Pseudomonas aeruginosa ATCC 10145 were used to determine the antimicrobial effects, minimum inhibitory concentration (MIC) and minimum bactericidal concentration (MBC) of the iron oxide nanoparticles as reported previously[24].

2.4.3. Mechanical resistance of coated epoxy/ iron oxide nanocomposites films

The mechanical properties of cured films on the steel panels were carried out according to appropriate ASTM standard test methods. More details about the mechanical properties of epoxy coatings were discussed in previous work [27]. The steel panels were blasted and cleaned according ASTM D 609-00. The DFT was measured according to ASTM D 1005-07. The adhesion pull-off test was evaluated according to (ASTM D 4541-02) using a hydraulic pull-off adhesion tester in the range of 0–25 MPa. The bend test was used to measure the film flexibility according (ASTM D 522-93a). The impact resistance used to evaluate the resistance of films to mechanical was evaluated using (ASTM D2794-04). The film hardness was evaluated by means of the pencil test (ASTM D 3363-00). The hardness was determined by using Erichsen hardness test pencil, model 318S, scratching force in the range of 0.5–20 N.

The abrasion resistance of epoxy cured films was evaluated according ASTM D4060-07 by applying 5000 cycles with 1000 g load on the tested panels.

2.5. Corrosion resistance of epoxy films

2.5.1 Salt spray resistance

A salt spray cabinet manufactured by CW Specialist equipment ltd. model SF/450, was used to evaluate the salt spray resistance of coated panels according to ASTM B117-03. The corrosion resistance was evaluated in terms of blistering, scribe failure and a degree of rusting, in relation to ASTM standards, i.e. ASTM D714-02, D1654-00 and D610-01 respectively.

2.5.2 Electrochemical Measurements

Electrochemical measurements were performed using Solartron 1470E (multichannel system) as electrochemical interface and the Solartron 1455A as Frequency response analyzer. EIS measurements were initiated applying to the electrode a sinusoidal amplitude of 10 mV on the frequency range from 10^4 to 10^{-2} Hz. Potentiodynamic polarization curves were recorded with a scan rate of 1 mV/ s.

3. RESULTS AND DISCUSSION

Passivation of carbon steel is one of the most important techniques used to control either atmospheric or wet corrosion problems [28]. Passivation describes the formation of stable ferric oxide layers on carbon steel to minimize the formation of ferrous rust from exposure to atmospheric corrosion. The formation of a solid uniform maghemite (γ -Fe_2O_3), produced from oxidation of ferrous cations into a ferric state, forms a strong passivity for steel. Magnetite and maghemite were preferred as part of the passivation process to protect the steel surfaces from further atmospheric corrosion. The dissolution of iron oxide (rust) in water activates the carbon steel surface and creates other corrosion problems elsewhere [28]. It was previously reported that magnetite can be converted to other oxide (rust) either in dry or wet atmosphere according to the following equations [29]:

$$2Fe^{2+}Fe_2^{3+}O_4(\text{magnetite}) + 1/2O_2 \longrightarrow 3\text{-}Fe_2^{+3}O_3(\text{hematite}) \quad (1)$$

$$Fe_2^{+3}O_3(\text{hematite}) + nH_2O \longrightarrow Fe_2O_3.nH_2O(\text{limonite}) \quad (2)$$

The sensitivity of magnetite or maghemite to water or oxygen can be controlled by particle size, shape and coating of magnetite nanomaterials with a suitable capping agents. The present work aims to prepare highly dispersed magnetite nanomaterials with controlled shape and size to disperse in epoxy resin as organic coatings for carbon steel. Moreover, the formation of undesirable oxide film on the carbon steel coated with cracked or damaged epoxy can be inhibited by release of magnetite from epoxy by capillary forces to act as self-healing for the uncoated carbon steel surface. The releasing of the magnetite nanoparticles into the environment is unavoidable [30, 31]. For this reason, the present work aims to prepare antimicrobial magnetite nanoparticles.

3.1. Characterization of iron oxide nanoparticles

In our previous works [26] the water soluble extract of Myrrh gum was used to prepare highly dispersed magnetite nanoparticles having uniform particle size distribution. The magnetite nanoparticles were prepared by a simple method with high yield by reacting ferric chloride with potassium iodide without removal of iodine in alkaline ammonium hydroxide solution pH 9 according to following equation [32]:

$$3FeCl_3 + KI + 8NH_4OH \longrightarrow Fe_3O_4 + \tfrac{1}{2} I_2 + 4H_2O + KCl + 8NH_4Cl \quad (3)$$

It was reported that the presence of iodine in the reaction mixture produced mixture of iron oxide based on magnetite and maghemite [26]. For this reason, the present work used Myrrh

water/ethanol soluble fraction as capping agent in the presence and absence of iodine to prepare capped iron oxide nanoparticles as described in the experimental section.

FTIR spectra of capped iron oxide nanoparticles in presence and absence of iodine were represented in Fig. 1 a and b, respectively. All spectra indicate the presence of band at 570 cm^{-1} (Fig. 1 a and b) that attributed to Fe-O stretching of magnetite. The appearance of new bands at 650 and 750 cm^{-1} in spectrum of iron oxide capped with Myrrh in presence of iodine indicates the presence of maghemite [26]. Moreover, the absence of broad intense band at 3450 cm^{-1} in all spectra confirms the absence of OH groups of α-Fe2O3 (hematite) nanoparticles [26]. The presence bands at 1630 and 1550 cm^{-1} in all spectra confirms the presence of -COOH and C=C stretching of Myrrh gum [26] that indicates the capping of iron oxide with Myrrh.

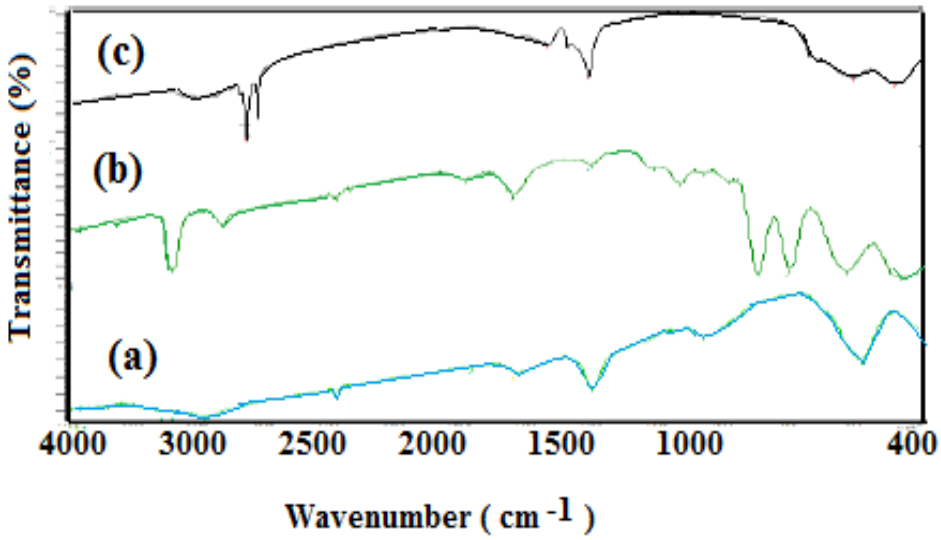

Figure 1. FTIR spectra of a) iron oxide/Myrrh, b) iron oxide/Myrrh/I_2, and c) damaged epoxy iron oxide/Myrrh/I_2 nanoparticles.

The composition of iron oxide nanoparticles capped with Myrrh in the presence and absence of iodine can be determined by XRD as represented in Fig. 2 a and b. The diffraction patterns of magnetite capped with Myrrh in absence of iodine (Fig. 2a) are identical to pure magnetite peaks (JCPDS No. 07-0322) that confirms the FTIR data. The diffraction peaks at (110), (220), (311), (400), (422), and (511), which are the characteristic peaks of the Fe_3O_4 crystal with a cubic spinal structure. The appearance of peak at 2-theta 41.3^o (Fig. 2b) confirms the presence of maghemite diffraction of (111) and indicates the presence of maghemite with magnetite and disappearance of hematite diffractions [26]. These data concluded that the iron oxide nanoparticles capped with Myrrh in the presence of iodine produced magnetite and maghemite nanoparticles while pure magnetite was produced by capping of magnetite with Myrrh and removal of iodine from the reaction medium.

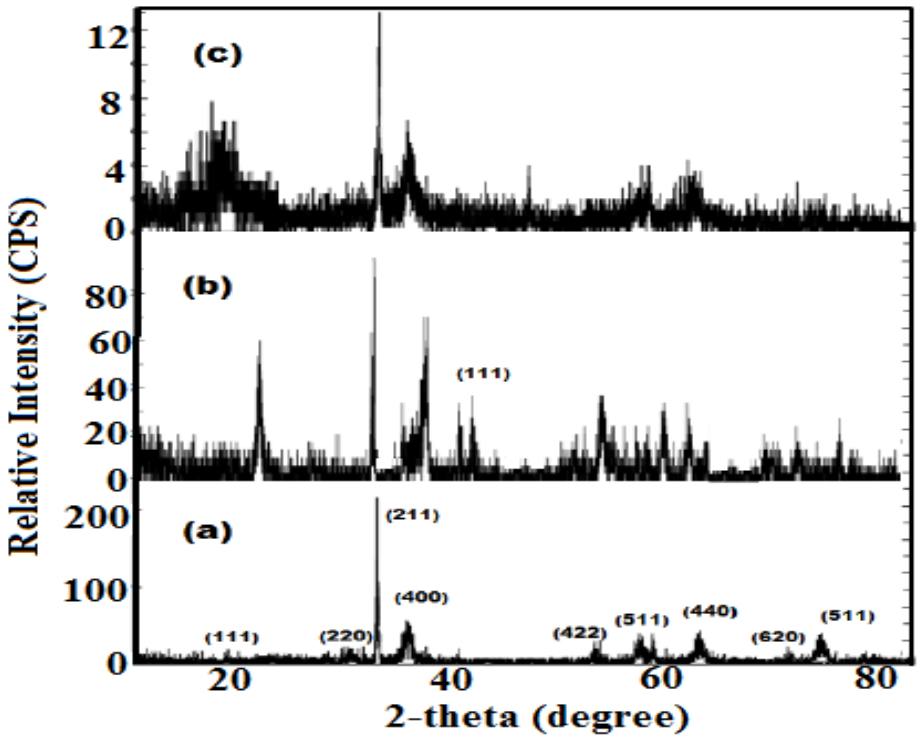

Figure 2. XRD diffractograms of a) iron oxide/Myrrh, b) iron oxide/Myrrh/I_2, and c) damaged epoxy iron oxide/Myrrh/I_2 nanoparticles.

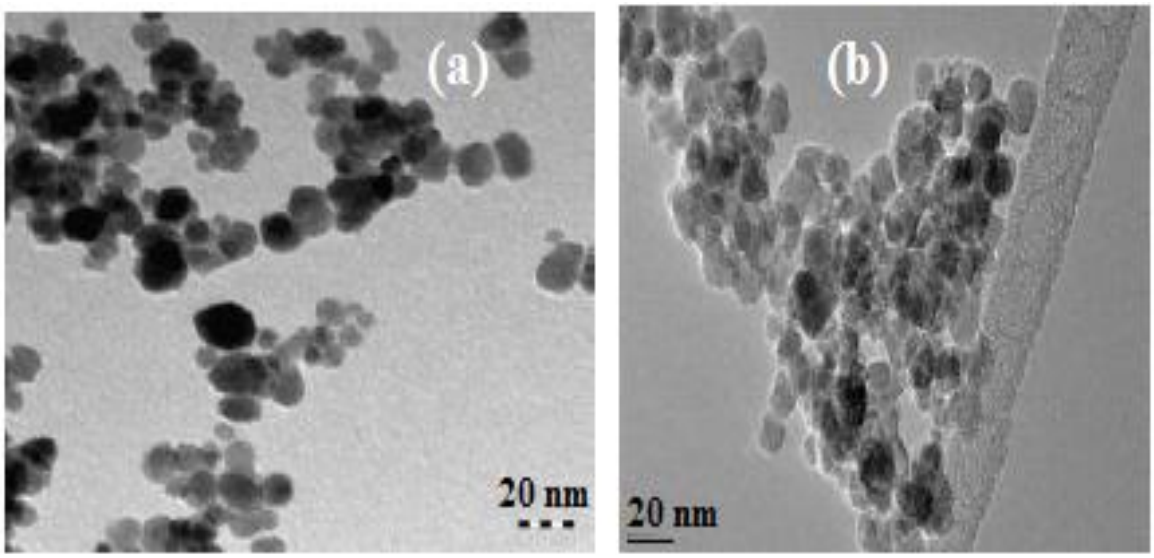

Figure 3. TEM micrographs of a) iron oxide/Myrrh, and b) iron oxide/Myrrh/I_2 nanoparticles.

The morphologies of the iron oxide nanoparticles capped with Myrrh in the presence or removal of iodine from reaction medium are illustrated from TEM micrographs as represented in Fig.3a and b. The micrographs indicate that the capped iron oxide nanoparticles with Myrrh have spherical shapes. Moreover, the particles form aggregates when the iodine removed from reaction medium. It is also observed that the presence of dark points inside the spherical particles indicates the

encapsulation of magnetite nanoparticles into the Myrrh to form nanocomposite. TEM images show core shell morphologies and confirm also that there is no iron nanoparticles formed without capping with Myrrh.

3.2. Antimicrobial activity

It is necessary to measure the antimicrobial activity of iron oxide nanoparticles capped with Myrrh before application as self-healing material for epoxy organic coatings of steel to detect their effects on the environments as described in the experimental section. The influence of iron oxide nanoparticles on micro-organisms is ambiguous. The antimicrobial activity of capped iron oxide nanoparticles with Myrrh in vitro level as described in the experimental section are evaluated and listed in Table 1. The data indicate that the iron oxide nanoparticles prepared without removal of iodine acheived good results with all tested bacterial strains. The MIC values were ranged from 5 to 10 $\mu g\ mL^{-1}$ that completely inhibited the growth of S. aureus *and* E coli. This means that the good dispersion of iron oxide nanoparticles increases their adsorption on the bacterial wall. The data represented here agree with other studies [33-35] which proved that iron oxide nanoparticles substantially inhibited the growth of E. coli and S. aureus due to their ability to absorb at interfaces and forming bio films at the nanoparticle surfaces [35].

Table 1. Antimicrobial activity MIC of Myrrh capped magnetite nanoparticles.

Antimicrobial materials		MIC ($\mu g\ mL^{-1}$)	The reduction of organism (%)			
			1 $\mu g\ mL^{-1}$	2.5 $\mu g\ mL^{-1}$	5 $\mu g\ mL^{-1}$	10 $\mu g\ mL^{-1}$
Iron oxide/Myrrh/I_2	E. coli	10	-	25±4	52±7	80±8
	S. aureus	5	25±3	45±5	85±7	95±4
	B. subtilis	-	-	-	-	-
	P. aeruginosa	-	-	-	45±7	65±7
Iron oxide/Myrrh	E. coli	-	-	-	-	-
	S. aureus	>10	-	37±8	63±5	75±4
	B. subtilis	-	-	-	-	-
	P. aeruginosa	-	-	-	-	-

3.3. Mechanical properties of Epoxy

Cured epoxy resins offer good protection for carbon steel due to their good adhesion beside they show special chemical characteristics such as absence of by-products or volatiles and low shrinkage during curing reactions [36]. However, the properties of cured epoxy resins such as low fracture toughness and cracks affected their performance. There are many approaches used to improve the epoxy performance using additives such as nano-fillers, rubber agents or modification of epoxy chemical structures [37, 38]. The main drawback of epoxy composites is weakness of mechanical

properties due to impact forces that produced cracks. In the present work, iron oxide nanoparticles capped with Myrrh are used for developing epoxy self-healing property. It is expected in the present system that the iron oxide nanoparticles can be chemically bonded with epoxy resin and polyamine hardener as illustrated in Scheme 1.

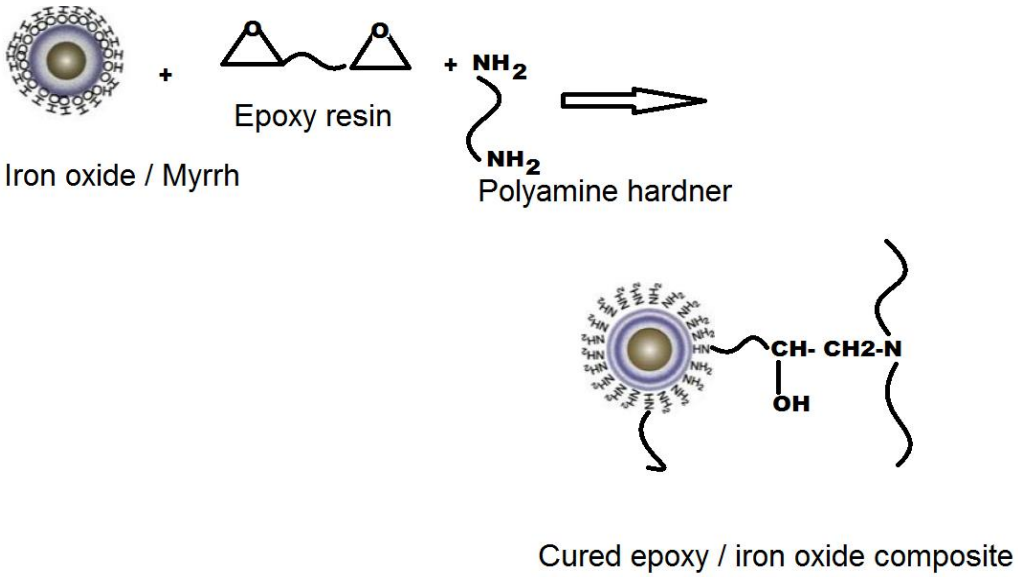

Scheme 1. Chemical interaction between iron oxide nanoparticles and two component epoxy system.

Table 2. Mechanical tests data of the cured epoxy iron oxide nanocomposites.

Nanoparticles %		Hardness (N)	Adhesion (pull off resistance) MP	T-bend	Impact (Joule)	Abrasion Resistance weight loss (mg)
blank		3	3	pass	5	65
Iron oxide/Myrrh/I_2	0.1	10	8	pass	12	19
	1.0	13	11	pass	14	14
	10	20	14	pass	18	9
Iron oxide/Myrrh	0.1	4	3	pass	7	40
	1.0	5	4	pass	9	35
	10	9	7	pass	10	28

FTIR spectra (Fig. 1) confirm the presence of hydroxyl groups due to presence of Myrrh (polysaccharide) and maghemite hydroxyl groups [26]. Moreover, the chemical interaction between hydroxyl groups of iron oxide nanoparticles and amine or epoxy groups of epoxy/hardener system introduces new shell based on amines or epoxy groups that reduce the formation of physical chain entanglements that could produce from epoxy/polyamine systems [39]. This will reflect on

enhancement of the mechanical properties of the modified epoxy resins with iron oxide nanoparticles. Accordingly, it is necessary to evaluate the mechanical properties of cured epoxy resins such as impact and abrasion resistances, hardness, bending and adhesion force with steel. The data of mechanical tests of cured epoxy resin in presence and absence of capped iron oxide Myrrh nanoparticles were determined and listed in Table 2 and represented in Fig. 4.

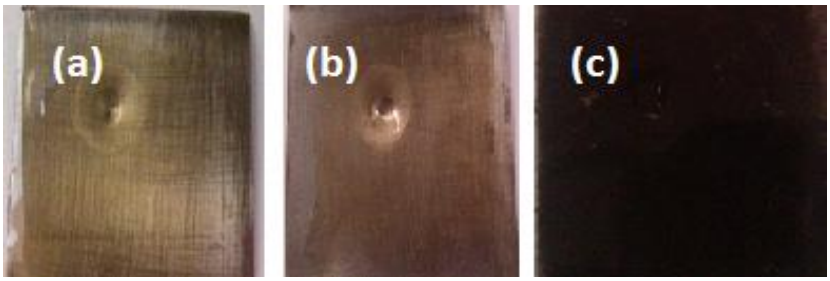

Figure 4. Impact resistance photo of epoxy using different weight contents of a) 0.1, b)1 and c) 10 Wt. % of iron oxide/Myrrh/I_2 nanoparticles.

The adhesion (pull-off test) of cured epoxy resins increased with increment of iron oxide capped with Myrrh in the presence of iodine contents more than magnetite capped with Myrrh in absence of iodine content. The superior adhesion of epoxy with steel capped with Myrrh in the presence of iodine confirms the good dispersability of iron oxide nanoparticles in the films and enhanced interaction between nanoparticles and epoxy polymer matrix that improve the mechanical and adhesion of epoxy with steel. The good nanoparticle dispersability leads to provide higher cross-linking density, improved thermal and chemical resistance properties of epoxies [40]. The increment of impact resistance of cured epoxy resins with increasing the iron oxide contents indicates the absence of any visual or internal cracks and formation of good adhered epoxy films with steel. Therefore, the intimate interaction between nanoparticles and epoxy polymer matrix reduces the impact stresses which transferred from the polymer matrix into the iron oxide nanoparticles. This good interaction between nanoparticles and epoxy system ensures a reduction of any internal crack propagation that occurs from curing of unmodified epoxy/polyamine system. This speculation can be confirmed from SEM of cured epoxy/iron oxide-Myrrh nanoparticles as illustrated in Fig.5. The SEM micrograph of unmodified epoxy resin (not represented for brevity) indicates smooth, glassy and homogenous microstructure. The SEM micrograph of cured epoxy/iron oxide-Myrrh nanoparticles (Fig. 5) shows good iron oxide nanoparticle dispersion even at high weight contents (10 Wt %) . Moreover, it confirms the absence of phase separation between nanoparticles and epoxy resins. The high dispersability of iron oxide nanoparticles among the networks confirms the good adhesion between iron oxide nanoparticles capped with Myrrh in the presence of iodine and epoxy resins. It was also observed that there is no any void formed (Fig. 5) which indicates the strong chemical interactions between iron oxide nanoparticles and epoxy system (scheme 1). Fig 5b confirms the formation of aggregates and iron oxide nanoparticles with poor dispersion in epoxy system. This reflects on the lowering mechanical properties when the iron oxide nanoparticles capped with Myrrh in absence of

iodine blended with epoxy due to lower adhesion between these nanoparticles and epoxy system. This can be referred to lower hydroxyl group contents surrounded iron oxide nanoparticles.

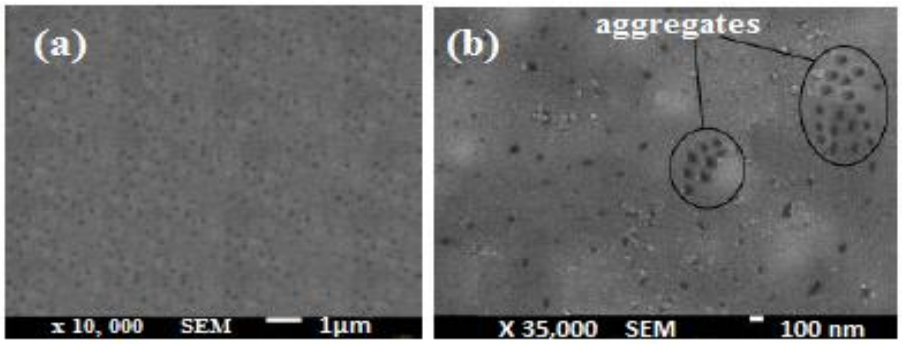

Figure 5. SEM micrographs of epoxy nanocomposites blended with 1 wt. % of a) iron oxide/Myrrh/I_2, and b) iron oxide/Myrrh nanoparticles.

3.4. Testing corrosion resistance of coating

The durability of epoxy resins as organic coatings for carbon steel can be estimated by evaluation of mechanical and corrosion tests. In the previous section we have estimated the mechanical tests of the cured epoxy with and without iron oxide nanoparticles. In the present section, we will estimate the corrosion resistance of the cured epoxy system using salt spray resistance and electrochemical tests.

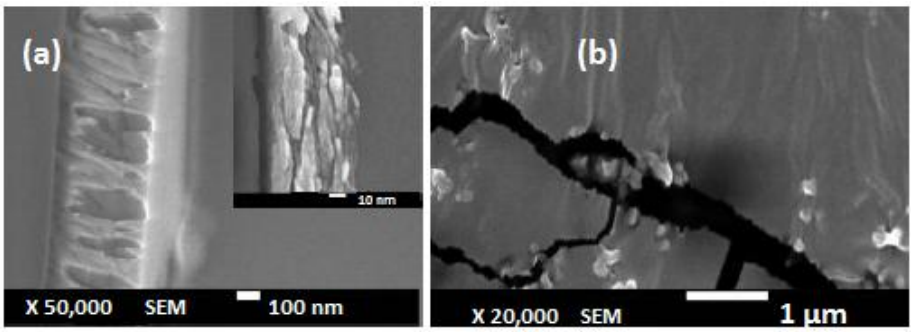

Figure 6. SEM images of damaged cured epoxy a) with 1 Wt % of iron oxide/Myrrh/I_2 nanoparticles and b) blank on steel panels.

In this section, the continuous salt spray cabinet, as illustrated in the experimental section, used to evaluate the effect of salt and humidity on the defected cured epoxy system coated on blasted and cleaned carbon steel panels. The duration times of tests were evaluated at the maximum 1000 hours recommended to the marine organic coatings. The disbanded area according to rust formation was measured as defected area to the total area of panel according to ASTM D1654. The results of salt spray test for cured epoxy system as blank and cured epoxy/iron oxide nanocomposites were listed in

Table 3. Moreover, the morphologies of the disbanded area of defects were represented in Fig.6 to estimate the self-healing properties of iron oxide nanoparticles.

The data, Table 3, indicate that the presence of iron oxide nanoparticles capped with Myrrh in the presence of iodine possess high salt spray resistances. It is well known from previous works [40-42] that the salt spray resistance increased with increasing the adhesion of substrate with coat which prevents the moisture vapor penetration through the coats, Moreover, it was reported that the production of more hydroxyl groups of the cured epoxy amine networks increased the adhesion of epoxy with steel [40].

Table 3. Salt spray resistance of the cured epoxy iron oxide / Myrrh nanocomposites.

Nanoparticles %		Disbonded area		Rating Number (ASTM D1654)
		cm^2	%	
blank		16.5	9	6
Iron oxide/Myrrh/I_2	0.1	1.6	1	9
	1.0	1.2	0.7	9
	10	0.5	0.1	10
Iron oxide/Myrrh	0.1	4.2	2.3	8
	1.0	3.1	1.7	9
	10	1.6	1	9

SEM image (Fig. 6 a) indicates the formation of rust and cracks of epoxy films without iron oxide nanoparticles. Fig. 6 b confirms the self-healing of iron oxide nanoparticles on the defect area of cured epoxy/iron oxide nanocomposites. The self-healing characteristics of iron oxide nanoparticles capped with Myrrh in the presence of iodine can be referred to their lower particle size can easily infiltrate the free-volumes of the epoxy networks; thus, the decrement of the free-volume of epoxy will lead to a further increase of self- healing of iron oxide to repair the defect coat area. The chemical structure and crystal structure of the materials formed at defected area are confirmed by FTIR and XRD as represented in Figs. 1c and 2c, respectively. The analyses confirm the presence of iron oxide nanoparticles (magnetite and maghemite without hematite) capped with Myrrh and epoxy on the defected area of steel.

3.5. Evaluation of corrosion resistance of epoxy nanocomposites.

3.5. 1. Open circuit potential (OCP) measurements

Fig. 7 shows the variation in open circuit potential of epoxy coated samples without and with iron oxide/Myrrh/I_2 nanoparticles as function of immersion time in 3.5 wt.% NaCl solution. The OCP values shifted to negative direction during the initial stage of immersion then gradually and slowly shifted to more positive values as immersion time elapsed during the last stage of monitoring. Fig. 7

displayed more positive OCP values of the epoxy coating samples with nanoparticles than the blank solution. The presence of high percent of nanoparticles causes a shift in potential to more positive OCP values compared to low percent of nanoparticles at all immersions times. It can be seen that there is a considerable difference in OCP value between blank and the epoxy samples containing nanoparticles. It can be stated that simultaneous penetration of oxygen and chloride ions through the scratched area enhances the steel corrosion. Therefore, active corrosion occurred and followed by gradual decreases of OCP values to negative direction during the initial stage of immersion. This result suggests that even in the presence of nanoparticles in the epoxy coating, active corrosion occurs under the coating layer during the initial immersion time. The nobler OCP value of epoxy coating containing nanoparticles can be attributed to the formation of protective layer, which lower and restrict the corrosive species access to the active sites of the coating surface in the 3.5 wt% NaCl solution. The protection action of the nanoparticles can be clearly seen from the ennobling the OCP values of the samples as shown in Fig. 7. The results indicated that the additions of nanoparticles to the epoxy coating enhanced the corrosion protection capabilities of the coating.

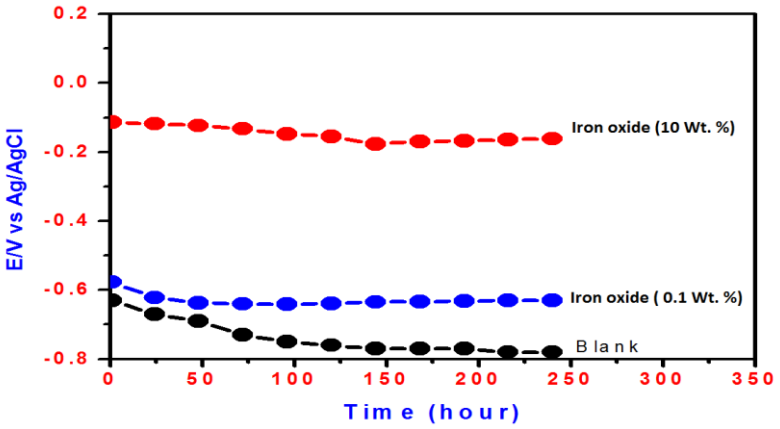

Figure 7. Influence of nanoparticle content on the OCP monitoring data for epoxy iron oxide/Myrrh/I_2coating nanocomposite on steel.

3.5.2. Potentiodynamics polarization measurements

Polarization curves of the epoxy coated samples without and with iron oxide / Myrrh / I_2 nanoparticles immersed in 3.5 wt.% NaCl solution were represented in Fig. 8. Tafel cathodic and anodic slopes (βa and βc; mV) and corrosion current density (I_{corr}; $\mu A/cm^2$) obtained by extrapolation of the Tafel are determined and summarized in **Table 4.** The data confirmed that the addition of the nanoparticles to the epoxy coating reduced the current densities of both anodic and cathodic polarization curves [43]. Also, the E_{corr} shifted toward more positive values for the samples containing nanoparticles. Results show that nanoparticles affect both the anodic and cathodic polarization curves more than experienced by the blank. However, the high percent of nanoparticles influenced the polarization curves more than lower one. The data presented in Table 4 show that the i_{corr} decreased in the presence of nanoparticles. It can be seen that the reduction in i_{corr} were most

pronounced for the specimens containing high percent of nanoparticles. It can be seen from the results that i_{corr} decreases with prolonged immersion times owing to the formation barrier film and causes a shift in the potential towards positive direction. The protection performance of the coating can be attributed to the formation of barrier film as a consequence of self-healing of the epoxy coating in presence of nanoparticles.

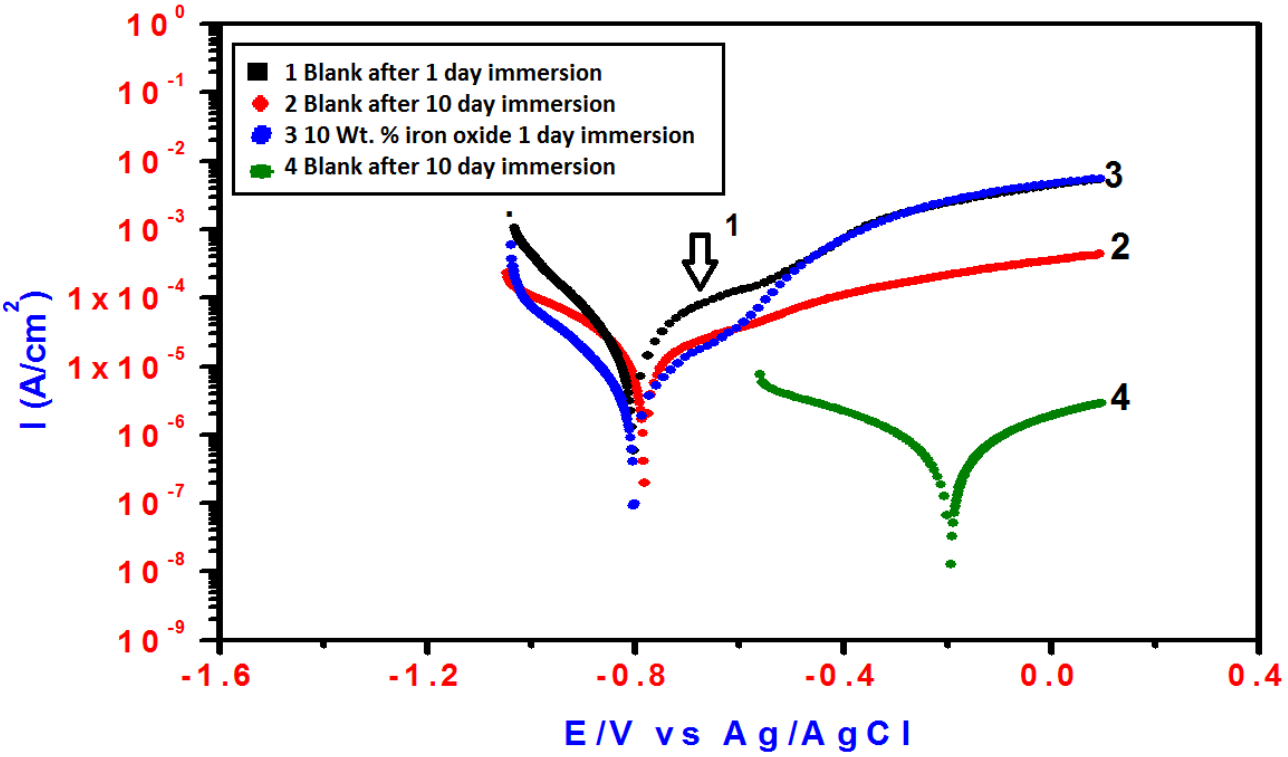

Figure 8. Influence of epoxy iron oxide/Myrrh/I_2coating nanocomposite on the polarization curves for the epoxy coating measured at different immersion times in 3.5% NaCl solution.

Table 4. Electrochemical parameters calculated by polarization and EIS methods at different immersion time.

System	Polarization Method				EIS Method
	βa (mV/decade)	βc (mV/decade)	E_{corr} (V)	$I_{corr,}$ μA/cm^2	R_p x10^5 Ohm
Blank after 1 day	193	356	-0.782	38.6	0.06186
Blank after 10 days	191	146	-0.805	17.7	0.09021
Epoxy nanocomposite with iron oxide/Myrrh/I2 after 1day	154	123	-0.802	2.94	0.73743
10 days	202	198	-0.19	0.322	0.92071

The protection performance of the coating can be attributed to the formation of barrier film as a consequence of self-healing of the epoxy coating in presence of nanoparticles. The addition of nanoparticles to the epoxy coating can also reduces the cathodic reaction by moving the potential towards positive direction due to limitation of the cathodic reaction, which results in raising its over voltage [44]. It can be concluded that the self-healing of the scratched area results in the formation of corrosion products, which acts as barrier film for access of the active species as chloride ions to attack the underlying substrate. These results clearly illustrate the corrosion protection performance of epoxy coating samples containing nanoparticles. The action of nanoparticles is due to their barrier properties, which limits the pathway whereby aggressive ions achieve the underlying substrate.

3.5.3 Electrochemical impedance spectroscopy (EIS) measurements

EIS was utilized in order to analyze the protection of the coating performance immersed in the 3.5% NaCl solution. Fig. 9. shows the Bode plots of the coating samples without and with nanoparticles at different immersion times. Results confirm that as immersion time increased the impedance of the coating samples containing nanoparticles increased. The difference in impedances measured at low and high frequencies was used to determine polarization resistance (Rp) [45]. Moreover, the difference in the modulus of impedance between the blank and coating samples containing nanoparticles increases with the immersion time. The increment of impedance was most pronounced in the presence of high percent of nanoparticles.

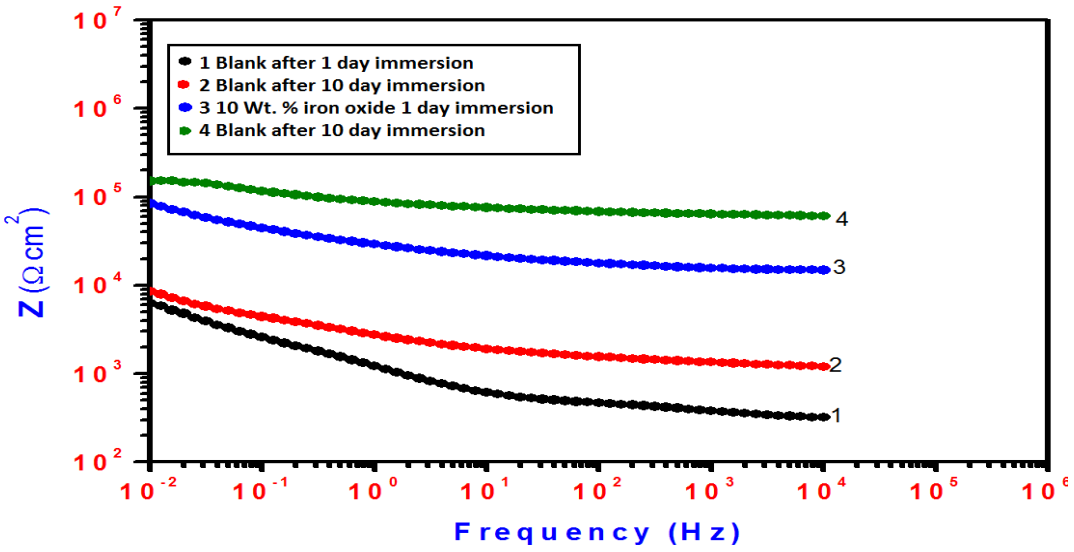

Figure 9. The Bode plots of epoxy coating with different percentages of iron oxide/Myrrh/I_2 nanoparticles at different immersion times in 3.5% NaCl solution.

A significant difference between the blank and coating samples containing nanoparticles was observed (Fig. 9) and suggesting that the nanoparticles increased the barrier properties of the coatings. The impedance at 10 mHz of the coating is also increased using nanoparticles. The increase of the impedance is more pronounced at 10 wt.%. It seems that the nanoparticles could efficiently restrict

the access of the aggressive ions to the underlying substrate surface through forming protective layer on the coating surface by self-healing of the scratched area. The highest polarization resistance (Rp) is reported for coating sample with highest percent of nanoparticles, while the lowest is experienced for blank sample. The penetration of the aggressive ions into the coatings through the scratched area makes the coating resistance diminished. The gradual penetrating of the aggressive ions during the initial stage of immersion results in increasing the active area and more aggressive species reach the surface. At this condition, the corrosion process of the substrate beneath the coating layer is facilitated and enhanced especially during the initial immersion. As the immersion time elapsed, a significant improvement in coating protection is detected due to formation of barrier film by self-healing of the scratched area of the coating samples with nanoparticles. Also with releasing the corrosion products, coating samples with nanoparticles can form corrosion products underneath the coating and protect the underlying substrate surface. The additions of nanoparticles to the epoxy coating enhance the ability of the coating to create a protective layer on the underlying surface by self-healing. Therefore, the protection performance of the coating is increased. The increment of the percent of nanoparticle contents in the epoxy coating increases the self-healing of the coating for formation the barrier layer. It can be also concluded that a barrier layer was released after scratching the coating containing nanoparticles, which limited the access of the aggressive ions to attack the underlying substrate and provided more protection performance of the coating by self-healing effect.

By comparing the antimicrobial activity and the mechanical properties of the epoxy modified iron oxide / Myrrh / I_2 nanocomposite with previous work for addition of iron oxide capped with rosin amino-amidoxime [46], it was found that the mechanical properties such as abrasion resistance was increased by capping of iron oxides with Myrrh more than rosin amino-amidoxime. Moreover, the corrosion resistance of epoxy coatings in sodium chloride solutions was increased for epoxy networks embedded with iron oxide / Myrrh / I_2 nanoparticles more than that cured with iron oxide capped with rosin amino-amidoxime due to improvement in the mechanical properties and salt spray resistance. It was also noticed that the interaction between iron oxide nanoparticles and epoxy networks increases the corrosion resistance of the system more than individual magnetite nanoparticles that used as anticorrosive materials for steel in acidic medium [20-26].

4. CONCLUSIONS

New antimicrobial iron oxide nanoparticles capped with natural product of Myrrh gum were prepared with high yield. The iron oxide nanoparticles show strong interaction with epoxy cured amine system and enhance the adhesion and mechanical characteristics of epoxy nanocomposite films on the steel surfaces. The inclusion of small concentrations (0.1%) of iron oxide NPs can significantly enhanced the mechanical properties such as bending, abrasion and hardness of the nanocomposites because of well dispersion of iron oxide into epoxy composites and their chemical interactions with epoxy amine system. The additions of iron oxide nanoparticles to the epoxy coating provides more protection performance of the coating by self-healing effect. A barrier layer was released after scratching the coating containing nanoparticles, which limited the access of the aggressive ions to attack the underlying substrate. Epoxy nanocomposite coatings achieved higher corrosion resistance

to salt or marine environment than the other epoxy coating without iron oxide nanoparticles. The polarization data showed that the corrosion rate decreased in the presence of nanoparticles and the decrease in corrosion rate was most pronounced for the specimens containing high percent of nanoparticles. The nobler OCP value of epoxy coating containing nanoparticles can be attributed to the formation of protective layer, which restricted the corrosive species access to the active sites of the coating surface. The results obtained from the present investigation revealed that the presence of iron oxide nanoparticles based on magnetite and maghemite in the epoxy matrix endows it with various properties that make the epoxy nanocomposite a promising candidate as an self-healing and antimicrobial environmentally friendly organic coating epoxy for steel.

ACKNOWLEDGEMENT
The authors extend their appreciation to the Deanship of Scientific Research at King Saud University for funding this work through research group no RGP- 235.

References

1. M.V. Manuel, Principles of self-healing in metals and alloys: an introduction, In: S.K. Ghosh (ed.), *Self-healing materials: fundamentals, design strategies, and applications*, Wiley, Weinheim/New York (2009) 251–266.
2. J. Buha, R.N. Lumley, A.G. Crosky and K. Hono, *Acta. Mater*., 2007; 55: 3015-3024.
3. S .Wang and L. Jiang, *Adv. Mater*., 19 (20070 3423–3424.
4. M. Manuel and G.B. Olson, *Proceedings of 2nd International Conference on Self-healing Materials*, Chicago, (2009).
5. X. Chen, M.A. Dam, K. Ono, A. Mal, H.v Shen, S.R. Nutt, K. Sheran and F. Wudi, *Science,* 295 (2002) 1698–1702.
6. X. Chen, F. Wudl, A.K. Mal, H. Shen and S.R .Nutt, *Macromolecules,* 36 (2003) 1802–1807.
7. C. Dry, *Int. J. Modern. Physics. B.*, 6 (1992)2763–2771.
8. C. Dry, *Compos. Str.*, 35 (1996) 263–269.
9. X.P. Zhao, *Chinese Journal of Materials Research (in Chinese*), 10 (1996), 101–104.
10. D.Y.WU, S. Meure and D. Solomon, *Prog. Polym. Sci.*, 33 (2008) 479–522.
11. J. Asadi, N.G. Ebrahimiv and M. Kashani, *Composites: Part A : Appl. Sci. and Manufacturing*, 68 (2015) 56–61.
12. S. Meure S, D.Y.Wu and S.A.Furman, *Vib. Spectroscopy,B*, 52 (2010) 10–15.
13. S. Meure, R.J. Varley, D .Y. Wu, S. Mayo, K. Nairn and S. Furman, *Eur. Polym. J* ., 48 (2012) 524-531.
14. A.C. Balazs, *Materials today,* 10 (2007) 18-23.
15. J. Telegdi, T. Szabo, L. Romanszki and M. Paval, The use of nano-/microlayers, self-healing and slow-release coatings to prevent corrosion and biofouling, In *Handbook of Smart Coatings for Materials Protection*, Woodhead Publishing: Cambridge, UK, chapter7 (2014)0 pp 135-172.
16. D.V. Andreeva and D.G. Shchukin, *Materials today*, 11 (2008) 24-30.
17. B. Wetzel, P. Rosso, F. Haupert and K. Friedrich, *Eng. Fract .Mech*., 73 (2006)2375-2398.
18. S.R. White, N.R. Sottos, P.H. Geubelle, J.S. Moore, M.R. Kessler, S.R. Sriram, E.N. Brown and S. Viswanathan, *Nature*, 409 (2001) 794-797.
19. M.G. Ahangari and A. Fereidoon, *Mat. Chem. Phys.*, 151 (20150 112-118.
20. S.M.A. Hosseini, A.H. Jafari and E. Jamalizadeh, *Electrochim. Acta*, 54 (2009) 7207–7213.
21. G.A. El-Mahdy, A.M. Atta, H. A. Al-Lohedan, *J. Taiwan Instit. Chem. Eng.*, 45 (2014) 1947–1953.

22. A.M . Atta, O.E. El-Azabawy, H.S. Ismail, M.A. Hegazy, *Corros. Sci.,* 53 (2011) 1680–1689.
23. A.M . Atta, G.A. El-Mahdy, H.A. Al-Lohedan , A.M. El-Saeed, *Molecules*, 20 (2015) 1244-1261.
24. A.M . Atta, G.A. El-Mahdy, H.A. Al-Lohedan and S.A. Al-Hussain, *Int. J. Mol. Sci.*, 15 (2014) 6974-6989.
25. A.M . Atta, H.A. Al-Lohedan, S.A. Al-Hussain, *Int. J. Mol. Sci*., 16 (2015) 6911-693.
26. A.M . Atta, H.A. Al-Lohedan and S.A. Al-Hussain, *Molecules*, 19 (2014) 11263-11278.
27. A.M . Atta, Abdoua MI, Elsayed AA, Ragab ME, Prog Org Coat 2008; 63 : 372–376.
28. J.Y. Park, D. Patel, E.S. Choi, Baek MJ, Y. Chang, T.J. Kim, J.H. Lee, *Coll. Surf. A: Physicochemical and Eng. Aspects*, 367 (2010) 3 41–46.
29. J.D. Hu, Y. Zevi, X.M. Kou, J. Xiao, X.J .Wang and Y. Jin, *Science of the Total Environment*, 408 (2010) 3477–3489.
30. P. Guardia, B.B. Brugal, A.G. Roca, O. Iglesias, M.P. Morales, C.J. Serna, A. Labarta and X. Batlle, *J. Magn. Magn. Mater.*, 316 (2007) 756–759.
31. G. Oberdorster, E. Oberdorster and J. Oberdorster, *Environ. Health Perspect.*, 113 (2005) 823–39.
32. A.M. Atta , Z.F. Akl, *Mat. Chem. Phys.*, 163 (2015) 253-261.
33. A.M. Prodan, S.L. Iconaru, C.M. Chifiriuc, C. Bleotu, C.S. Ciobanu, M. Heino, S. Sizaret and D. Predoi, *J. Nanomaterials*, Article ID 893970(2103) 7 pages,http://dx.doi.org/10.1155/2013/893970
34. C. Chiiriuc, V. Lazar, C. Bleotu, I. Calugarescu, A.M. Gruezescu, D.E. Mihaiescu, D.E Mogosanu, A.S. Buteica and E. Buteica, *Dig. J. Nanomat. Biostr*., 6 (2011) 37–42.
35. W.C. Miles, P.P. Huffstetler, J.D. Goff and A.Y. Chen, *Langmuir*, 27 (2011) 5456–5463.
36. W. Keyoonwong, Y. Guo, M. Kubouchi, S. Aoki and T. Sakai, *Int. J. Corros*., 2012 (2012) 1-11.
37. B. Qi, Q.X. Zhang, M. Bannister and Y.W. Mai, *Compos. Struct.*, 75 (2006) 514–519.
38. B.C. Kim, S.W. Park and D.G. Lee, *Compos. Struct*., 86 (2008) 69–77.
39. M. Nickels, J. Xie, J. Cobb, J.C. Gore and W. Pham, *J. Mater.Chem.*, 20 (2010) 4776–4780.
40. M. Sangermano, A. Priola, G. Kortaberria, A. Jimeno, I. Garcia, I. Mondragon and G. Rizza, *Macromol. Mater. Eng.*, 292 (2007) 956–961.
41. A.M. Atta, A.F. El-Kafrawy, M.H. Aly and A.A. Abdel-Azim, *Prog. Org. Coat.*, 58 (2007) 13–22.
42. A.M. Atta, N.O. Shaker, M.I. Abdou and M. Abdelfatah, *Prog. Org. Coat*., 56 (2006) 91–99.
43. X. Shi, T.A. Nguyen, Z. Suo, Y. Liu and Avci R, *Surf. Coat. Technol.*, 204 (2009) 237–245.
44. I.N. Putilova, S.A. Balezin and V.P. Barannik, *J. Electrochemi. Soc*., 108(1961) 234C.
45. A. Yabuki and K. Okumura, *Corros. Sci.*, 59 (2012) 258–262.
46. A.M . Atta, A.M. El-Saeed, G.A. El-Mahdy and H.A. Al-Lohedan, *RSC Advances*, 5 (2015) 101923–101931.

© 2016 The Authors. Published by ESG (www.electrochemsci.org). This article is an open access article distributed under the terms and conditions of the Creative Commons Attribution license (http://creativecommons.org/licenses/by/4.0/).